Science Advances AAAS Research Article

TITLE

Dorsal-ventral patterned neural cyst from human pluripotent stem cells in a neurogenic niche

AUTHORS

Y. Zheng[1,2,†], X. Xue[1,†], A. M. Resto Irizarry[1], Z. Li[1], Y. Shao[1], Y. Zheng[1], G. Zhao[2,3] *, and J. Fu[1,4,5] *

AFFILIATIONS

[1]Department of Mechanical Engineering, University of Michigan, Ann Arbor, MI 48109, USA.

[2]Center for Biomedical Engineering, Department of Electronic Science and Technology, University of Science and Technology of China, Hefei 230027, Anhui, China.

[3]Anhui Provincial Engineering Technology Research Center for Biopreservation and Artificial Organs, Hefei 230022, Anhui, China.

[4]Department of Cell and Developmental Biology, University of Michigan Medical School, Ann Arbor, MI 48109, USA.

[5]Department of Biomedical Engineering, University of Michigan, Ann Arbor, MI 48109, USA.

[†]These authors contributed equally to this work.

*Correspondence to: jpfu@umich.edu; zhaog@ustc.edu.cn.

ABSTRACT

Despite its importance in the central nervous system development, the development of the human neural tube (NT) remains poorly understood, given interspecies divergence and challenges of studying human embryo specimens. Here we report a human NT development model, in which NT-like tissues, termed neuroepithelial (NE) cysts, are generated in a bioengineered neurogenic environment through self-organization of human pluripotent stem cells (hPSCs). NE cysts correspond to the neural plate in the dorsal ectoderm layer and possess a default dorsal identity. Dorsal-ventral (DV) patterning of NE cysts is achieved using retinoic acid and/or Sonic hedgehog, featuring sequential emergence of the ventral floor plate, P3 and pMN domains in discrete, adjacent regions and an dorsal territory progressively restricted to the opposite dorsal pole. Together, this study reports the development of a hPSC-based, DV patterned NE cyst system for modeling human NT development, useful for understanding the self-organizing principles that guide NT patterning and hence to study neural development and disease.

INTRODUCTION

Neurulation is the embryonic process that begins with the specification of the neural plate containing neuroepithelial (NE) cells at the dorsal ectoderm germ layer, which then folds in upon itself towards the dorsal side of the embryo to form a tubular structure, the neural tube (NT), enclosing a central fluid-filled lumen. The posterior region of the NT gives rise to the spinal cord, whereas the anterior region becomes the brain, which together comprise the central nervous system (CNS). A very important process during neurulation is the progressive specification of the NT along the dorsal-ventral (DV) axis, that's, DV patterning of the NT (*1, 2*), which leads to the differentiation of distinct classes of neuronal progenitor cells located at defined positions within the NT. In recent years, tremendous progress has been achieved in understanding the molecular mechanism(s) of DV patterning of the NT using model organisms. It becomes appreciated that the allocation of neuronal fate in the NT is directed by secreted inductive factors (*i.e.*, morphogens) emanated from local surrounding tissues (*1, 2*). Thus, the position of progenitor cells in the NT influences their fate by defining the identity and concentration of inductive signals to which they are exposed. However, in the ultimate quest to understand the mechanism(s) of human NT development with the goal to prevent and treat developmental defects in the human CNS, studies using model systems remain suboptimal, given significant interspecies divergence (*3*). This limitation is further compounded by limited accessibility to the *in utero* post-implantation mammalian embryo for experimental studies.

Human pluripotent stem cells (hPSCs), including human embryonic stem cells (hESCs) and induced pluripotent stem cells (hiPSCs), have been successfully utilized for modelling post-implantation human embryonic development (*4-9*). These stem cell-based human development models provide promising experimental systems to study early neural development in humans, as neural cells derived *in vitro* from hPSCs display molecular and functional properties compatible to those in the developing embryonic brain (*10*). Technological advances in three-dimensional (3D) hPSC cultures have further led to the development of self-organized, multicellular neuronal tissues, termed brain organoids, that resemble the cerebral cortex, midbrain, and many other brain regions (*11*). Importantly, a 3D, DV patterned NT model has recently been reported in a pioneering work with mouse ESCs (*12, 13*). However, progress in generating a stem cell-based, DV patterned human NT model has been limited. A recent work shows 3D induction of dorsal, intermediate and ventral spinal cord-like tissues from hPSCs in a free-floating cell aggregate culture system (*14*). However, this work falls short in demonstrating fully organized patterning of spinal cord-like tissues along the DV axis. The apical surface of spinal cord-like tissues derived in this work faces outside external environments (*14*), distinctly different from the NT *in vivo*. Together, it remains elusive whether hPSCs can be utilized to generate a human NT development model with full DV patterning.

In this work, we sought to develop a biomimetic 3D culture system mimicking the *in vivo* neurogenic niche for the development of a hPSC-based, DV patterned human NT development model. The biomimetic 3D culture incorporates some key *in vivo*

neurogenic niche elements (*15*), including a 3D basal lamina extracellular matrix (ECM) to provide a permissive extracellular environment and a soft tissue bed to reconstruct the mechanical environment provided by the ventricular surface and ECM for the neuroepithelium during neurulation. This 3D biomimetic culture system allows for convenient manipulations of dynamic interplays between chemical and biophysical signals that are critical for the cellular morphogenetic events and progressive neuronal fate specification during DV patterning of NT-like tissues derived from hPSCs. Development of the biomimetic 3D culture system, together with extrinsic exogenous biochemical signals delivered at precise timing and concentration, allows us to apply hPSCs to achieve the development of a human NT development model with full DV patterning. Our hPSC-based *in vitro* NT development model provides a valuable experimental tool for the analysis of human NT development and will contribute to researches on NT-related diseases and potentially to drug discovery and regenerative medicine.

RESULTS

3D biomimetic culture for neuroepithelial cyst development

In the 3D biomimetic culture system, H9 hESCs were plated as single cells at 50×10^3 cells cm^{-2} onto a thick, soft gel bed of Geltrex (with thickness $\geq$ 100 μm, bulk *Young*'s modulus $\sim$ 900 Pa, coated on a glass coverslip), in mTeSR1 medium supplemented with the ROCK inhibitor Y27632 (**Fig. 1A&B**). At 24 h (day 1), a neurogenic environment was established by replacing mTeSR1 with a fresh neural induction medium comprising N2B27 supplemented with SB431542 (SB, TGF-β inhibitor) and LDN 193189 (LDN, BMP4 inhibitor) (*16, 17*) (**Fig. 1A&B**). To establish a 3D neural induction environment, 2% (*v* / *v*) Geltrex was further supplemented into the neural induction medium (hereinafter referred to as 'Gel-3D'; **Fig. 1A&B**). To assess the effects of ECM dimensionality and matrix rigidity, different modifications of the Gel-3D culture were conducted (**Fig. 1B**). First, glass coverslips coated with the soft gel bed were substituted with coverslips pre-coated with a thin layer of 1% Geltrex (hereinafter referred to as 'Glass-3D'; **Fig. 1B**). Second, the 3D ECM overlay in Gel-3D was removed from the neural induction medium, with the gel bed retained on coverslips (hereinafter referred to as 'Gel-2D'; **Fig. 1B**). Finally, a standard 2D culture using glass coverslips pre-coated by 1% Geltrex was utilized (hereinafter referred to as 'Glass- 2D'; **Fig. 1B**).

Under neural induction condition in Glass-2D, hESCs exited pluripotency and differentiated into NE cells, evidenced by strong expression of PAX6, an early neuroectodermal marker, by day 8 (**Fig. 1C&D**). Immunostaining and immunoblotting of N-CADHERIN (N-CAD) at day 8 further confirmed successful neural conversion in Glass-2D (**Fig. 1C** and **Fig. S1A&B**). Confocal images recorded at day 8 show localized N-CAD expression at the top surface of NE cells in Glass-2D (**Fig. S1A**), suggesting formation of the apical surface facing culture medium and the basolateral surface facing coverslip. Strikingly, in both Glass-3D and Gel-3D, while undergoing

neural conversion with upregulated PAX6 expression, hESCs self-assembled to form pseudostratified, multicellular cystic tissues enclosing a central lumen with the N-CAD+ apical surface facing inward (**Fig. 1C&D**). The lumenal NE cyst in Glass-3D featured a flattened, pancake-shaped morphology, with a jagged outside surface accommodating expanding NE cells along the apical-basal axis (**Fig. 1C** and **Fig. S1A**). In contrast, regular, spherical cystic tissues containing multilayered NE cells with smooth outside surfaces were evident in Gel-3D (**Fig. 1C&D**). In Gel-2D, even though hESCs clustered together as in Glass-3D and Gel-3D, the multicellular structures became irregular and discontinuous, with much fewer cells expressing PAX6 or N-CAD by day 8 (**Fig. 1C** and **Fig. S1A&B**), suggesting that Gel-2D was not as conductive as Glass-2D, Glass-3D or Gel-3D for neural conversion. In Gel-2D, cystic tissues with irregular contour and elliptical contour constituted 63.01% ± 1.79% and 36.99% ± 1.79%, respectively, of all cystic tissues at day 8. The percentage of discontinuous cysts (cysts in which cells were missing in some areas) was 73.09% ± 2.20%. Moreover, multicellular structures in Gel-2D were smaller in size compared with those in Glass-2D, Glass-3D or Gel-3D (**Fig. 1C** and **Fig. S1A&C**). We next investigated the development of NE cysts in Gel-3D with different gel bed thicknesses (**Fig. S1D**). When the gel bed thickness decreased from 100 μm to 60 μm or 20 μm, which increased the effective substrate rigidity (*18*), although PAX6 expression was evident in all cysts, these cysts showed a flattened morphology with a jagged basal surface, similar to those cultured in Glass-3D (**Fig. S1D**). Altogether, our data suggest that matrix rigidity might be an important factor mediating the formation of spherical NE cystic tissues.

Additional molecular characterizations were conducted for lumenal NE cysts derived from H9 hESCs in Gel-3D. In addition to PAX6, NE cysts showed strong expression of SOX2 and NESTIN, another two neuroectodermal markers, at day 8. Neither SOX17, a definitive endoderm marker, nor BRACHYURY, CDX2 or EOMES, which are primitive streak and mesodermal markers, was detectable at day 8 (**Fig. 1D** and **Fig. S1E**), excluding mesoderm or endoderm lineages in Gel-3D. SOX1, another neuroectodermal marker, was not detectable at day 8 (data not shown). However, continuous culture for another 5 d promoted SOX1 expression (**Fig. 1E**). Thus, PAX6 expression preceded SOX1 during the progressive development of NE cysts in Gel-3D, consistent with previous studies of neuroectodermal tissue developments from hPSCs *(19)* and human embryonic tissues (*20*). Further examination of ZO-1, a tight junction protein and apical polarity marker, confirmed the apical surface facing the central lumen in NE cysts (**Fig. 1E**). During the NT development *in vivo*, neural progenitor cells in the pseudostratified neuroepithelium undergo interkinetic nuclear migration (*15*), which results in mitotic cells localized at the apical surface and nuclei undergoing DNA synthesis (S phase) displaced more basally. Indeed, immunostaining for EdU and phospho-histone H3 (pH3; a specific marker for mitosis (*11*)) at day 8 revealed that EdU labeled S-phase nuclei were preferentially located at the basal surface, whereas pH3+ mitotic cells were located closer to the apical surface (**Fig. 1F**).

Progressive neural conversion in Gel-3D

We next examined dynamic progressive development of lumenal NE cysts from H9 hESCs in Gel-3D. After initial cell seeding onto the gel bed, single H9 hESCs soon clustered together and formed individual small colonies (**Fig. S2A&B**). Soon after 3D ECM overlay was added at day 1, hESC colonies initiated the lumenogenesis program (*21*) and resolved into lumenal cystic tissues while undergoing neural conversion. Within each well of a 24-well plate, 101.33 ± 1.67 individual NE cysts were formed by day 8. Multicellular cystic tissues in Gel-3D displayed rapid growth from day 1 to day 8, resulting in a 90-fold increase in their projected area over the 8-day period (**Fig. S2C**).

Immunofluorescence analysis revealed that the exit of pluripotency and neural conversion of hESCs in Gel-3D occurred in a progressive, concurrent fashion (**Fig. S2D**). Notably, all lumenal cysts retained strong expression of OCT4 but without detectable PAX6 or N-CAD till day 4 (**Fig. S2D&E**). Emergence of PAX6 expression with concurrent loss of OCT4 was evident in a subset of lumenal cysts at day 6 (**Fig. S2D&E**). Specifically, at day 6, 16.50 ± 2.81% of lumenal cysts contained both OCT4+ and PAX6+ cells (**Fig. S2D&E**), suggesting neural conversion in progress. The percentage of lumenal cysts containing both OCT4+ and PAX6+ cells increased to 43.61 ± 4.23% at day 8 before decreasing to 6.07 ± 3.71% at day 10. By day 10, 93.93 ± 3.71% of lumenal cysts contained only PAX6+ NE cells without detectable OCT4+, suggesting completion of neural conversion (**Fig. S2D&E**). Western blotting for OCT4 and PAX6 at different days further confirmed the progressive, concurrent fashion of the exit of pluripotency and neural conversion of hESCs in Gel-3D during NE cyst development (**Fig. S2F**).

Default dorsal identity of neuroepithelial cysts

After specification of the neuroectoderm at the dorsal ectoderm germ layer, development of the CNS continues with the acquisition of dorsal neural identity, revealed by expression of dorsal markers such as PAX3, PAX7 and MSX1/2 (*14, 22, 23*), by the midline dorsal ectodermal cells of the gastrulating embryo. Studies using mouse ESCs also show the default dorsal neural identity of NE cysts (*12*). We thus sought to examine the default dorsal or ventral fate of NE cysts developed in Gel-3D. Immunostaining revealed that NE cysts uniformly expressed PAX6 at day 9 (**Fig. 2A&B**). However, dorsal neural marker PAX3 or MSX1 was not detectable at this time point (**Fig. 2B**). Similarly, ventral neural markers FOXA2, OLIG2 or NKX2.2 was not detectable either at day 9 (**Fig. 2B**). NE cysts were further continuously cultured for another 9 d before immunofluorescence analysis to examine expression of dorsal and ventral neural markers. NE cysts at day 18 showed clear expression of PAX6, PAX3 and MSX1, with ventral neural markers FOXA2, OLIG2 or NKX2.2 remaining undetectable (**Fig. 2B**). Together, these data show the default dorsal neural identity of NE cysts derived from hESCs, supporting a highly conserved default dorsal neural identity of the NT for vertebrates including humans.

Neuroepithelial cysts are responsive to WNT and SHH signaling

Dorsalization of the NT *in vivo* is mediated by a conserved signaling network involving BMP and WNT signals emanated from the neighboring non-neural ectoderm and the roof plate (*1, 2, 24*). To investigate whether NE cysts in Gel-3D would respond to WNT signaling for dorsal patterning, CHIR99021 (CHIR), a GSK3 inhibitor that functions as a WNT activator, was supplemented in neural induction medium from day 4 to day 9 (**Fig. 2C**). Immunofluorescence analysis revealed that a majority of NE cysts at day 9 showed PAX3 and MSX1 expression (**Fig. 2D**), supporting the effect of WNT activation on dorsalizing NE cysts. CHIR stimulation resulted in a regression of PAX6 expression within a confined region at the center of NE cysts (**Fig. 2D**), resembling the dorsal to ventral shift of PAX6 expression in the chick NT under WNT stimulations (*25*).

A sonic hedgehog (SHH) signaling gradient anti-parallel the DV axis emanated from the notochord and the FP (FP) has been shown critical for ventral patterning of the NT (*1, 2, 24*). During early ventral patterning of the NT, SHH signaling subdivides ventral NE cells into three main domains, namely pMN, p3 and FP, along the DV axis (*1, 2, 24*). These ventral progenitor domains are identified by distinct transcription factors that further specify neuronal subtypes in each domain. The OLIG2+ pMN domain gives rise to motor neurons (MNs), whereas the NKX2.2+ p3 and FOXA2+ FP domains generate V3 neurons and a glial structure, respectively (*26*). Current protocols for ventralizing NE cells rely on morphogens including SHH and RA (*27*). To achieve ventral patterning of NE cysts in Gel-3D, we first activated SHH signaling by supplementing Smo agonist (SAG; 1 μM), an agonist of SHH signaling that functions by directly inhibiting Ptc, a receptor of SHH proteins, in neural induction medium from day 4 to day 9 (**Fig. 2C**). A few individual cells expressing OLIG2 and FOXA2 emerged sparsely in NE cysts at day 9 (**Fig. 2D**). However, NKX2.2 was not detectable at day 9 (**Fig. 2D**). We next added RA (1 μM) with SAG from day 4 to day 9. A significant increase of both OLIG2+ cells and FOXA2+ cells was evident at day 9 (**Fig. 2D**), consistent with the effect of RA on the acquisition of MN fate by NE cells (*28*). However, these OLIG2+ and FOXA2+ cells didn't emerge as distinct domains as *in vivo*, and NKX2.2+ cells remained undetectable at day 9 (**Fig. 2D**). To achieve induction of NKX2.2, we further added SHH proteins (10 nM) into neural induction medium already containing SAG and RA from day 4 to day 9. Under this enhanced ventralization condition, OLIG2+ cells and FOXA2+ cells further increased their numbers at day 9 (**Fig. 2D**). Excitingly, sparsely distributed NKX2.2 cells emerged in NE cysts (**Fig. 2D**). Together, these data suggest that specification of OLIG2+ pMN progenitor cells and FOXA2+ FP cells precedes the induction of NKX2.2 p3 progenitor cells in Gel-3D.

DV patterning of neuroepithelial cysts

Our data in **Fig. 2** showed that even though pMN, p3 and FP progenitor cells were induced by RA, SAG and SHH in Gel-3D by day 9, ventral patterning of NE cysts with properly aligned pMN, p3 and FP domains was not achieved. To determine whether Gel-3D could support DV patterning of NE cysts, culture time was prolonged to 18

days, with RA (1 μM) and SAG (1 μM) or RA (1 μM) and SHH (either 10 nM or 100 nM) supplemented into neural induction medium from day 4 to day 9 (**Fig. 3A**). Indeed, with RA and SAG, a small portion of NE cysts (< 5%) displayed the key architectural feature of DV patterning at day 18, with ventral progenitor domains aligned adjacent to an induced FP region (**Fig. 3B&C**). Specifically, in these patterned NE cysts, a single FOXA2+ FP domain emerged asymmetrically at one pole of the cyst (**Fig. 3B**). Adjacent to the FP, two NKX2.2+ p3 progenitor domains emerged in a symmetrical fashion (**Fig. 3B**). Two OLIG2+ pMN domains also simultaneously emerged dorsal to the two NKX2.2+ p3 domains, respectively (**Fig. 3B**). Importantly, by day 18, PAX3+ dorsal NE cells became detectable and were restricted to the opposite pole of the OLIG2+ pMN domain (**Fig. 3B**), suggesting successful DV patterning of NE cysts under RA and SAG stimulation. The percentage of DV patterned NE cysts was significantly increased with SAG replaced with SHH. With RA and 10 nM SHH, a significant percentage of NE cysts (22 ± 3.06%) displayed DV patterning at day 18 (**Fig. 3D & Fig. S3**). It is worth noting that under this condition, a majority of patterned NE cysts contained only one FP domain, with only 8.69% ± 0.66% of patterned NE cysts contained two FOXA2+ FP domains (**Fig. S4A&B**). In addition, the ventral pole of DV patterned NE cysts where the FOXA2+ FP was located appeared much thinner compared to other regions of the same NE cyst (**Fig. S4C&D**). In contrast, the thickness of unpatterned NE cysts was uniform along the cyst periphery (**Fig. S4C&D**). This observation is consistent with earlier reports showing that nuclei in the FP region are accumulated towards the basal surface (*12*) and high levels of SHH signaling inhibit proliferation (*29*), leading to a much thinner FP region in the NT.

We confirmed that spherical PAX6+ NE cysts containing single central lumens could be derived from H1 hESC line and a hiPSC line (1196a) in Gel-3D under neural induction condition by day 8 (**Fig. S5A&B**). With RA and 10 nM SHH treatment from day 4 to day 9, proper DV patterned NE cysts were also achieved using H1 hESC line and 1196a hiPSC line in Gel-3D at day 18 (**Fig. S5C-E**).

We further examined DV patterning with RA and 100 nM SHH (**Fig. 3E&F**). Under RA and 100 nM SHH, the percentage of ventral patterned NE cysts (27.03 ± 0.58%) with pMN and p3 progenitor domains properly aligned adjacent to an induced FP region was compatible to the value under RA and 10 nM SHH (**Fig. 3F**). However, very few PAX3+ dorsal cells were detected in NE cysts (**Fig. 3E**), suggesting an inhibitory effect of dorsal fate specification under this heightened ventralizing condition.

We next examined expression of other lineage markers associated with different ventral NT domains in NE cysts obtained under treatment with RA and 10 nM SHH (**Fig. S6A**). DBX1 (marker for p0 domain), DBX2 (marker for p0 and p1 domains), or NKX6.2 (marker for p1 domain) was not detectable at day 18 (data not shown). It is likely that induction of these more dorsally localized domains might require other morphogen signals such as BMP or WNT, which are secreted by tissues adjacent to the NT *in vivo*. Interestingly, around 20% of NE cysts showed localized expression of NKX6.1 (**Fig. S6B**), a marker for the p3, pMN and p2 domains (*30, 31*). The OLIG2+

pMN domain enclosed in the NKX6.1+ domain was observed in 22.27% ± 4.24% of NE cysts (**Fig. S6B&C**). We further observed mutually exclusive expression of NKX6.1 domain and FOXA2 domain in 13.6% ± 2.86% of NE cysts (**Fig. S6B&C**).

Progressive DV patterning of neuroepithelial cysts

We next studied dynamic, progressive DV patterning of NE cysts by tracking spatiotemporal expression of dorsal and ventral markers, with NE cysts stimulated with RA (1 μM) and SHH (10 nM) from day 4 to day 9 (**Fig. 4**). At day 9, all NE cysts contained PAX3+ dorsal cells but without any OLIG2+ pMN progenitor cells detectable (**Fig. 4A&B**). OLIG2+ cells started to emerge at day 12 in cyst regions where PAX3 expression was absent (**Fig. 4A**). From day 14 to day 18, the percentage of NE cysts containing OLIG2+ cells continued to increase, whereas the PAX3 domain continuously became more restricted (**Fig. 4A**). In a subset of NE cysts where OLIG2+ cells emerged as a cluster (the putative pMN domain) towards the prospective ventral pole of the cyst, concurrent, progressive restriction of the PAX3+ domain towards the opposite dorsal pole was evident (**Fig. 4A**), suggesting dynamic progression of DV patterning regulated by RA and SHH through dual effects on ventralization and antagonizing dorsalization (*32*). PAX3-OLIG2 DV polarity was established in 3.33% ± 1.33% of cysts at day 12, and this value increased at day 14 and day 16 and reached 26.52 ± 5.34% at day 18 (**Fig. 4A&B**).

We next tracked NKX2.2 and FOXA2 expression. At day 9, NKX2.2 was not detectable; but 65.35 % ± 2.79% NE cysts contained sparsely distributed FOXA2+ FP progenitor cells (**Fig. 4C&D**). At day 12, NKX2.2 remained undetectable; however, the percentage of NE cysts containing FOXA2+ cells decreased to 26.67% ± 1.76% (**Fig. 4C&D**). Notably, FOXA2+ cells appeared as a cluster (the putative FP domain) at the presumptive ventral pole at day 12 (**Fig. 4C&D**). NKX2.2 became detectable from day 14 onwards, and its expression was evident only in cysts containing FOXA2+ cells (there was < 4% cysts containing only NKX2.2+ cells at day 14; **Fig. 4C&D**). Importantly, 17.62% ± 2.23% of NE cysts at day 14 displayed localized NKX2.2 domains dorsal to the FOXA2+ FP region (**Fig. 4C&D**), suggesting dynamic patterning of ventral domains. The percentage of such ventral patterned NE cysts increased to 46.18% ± 1.95% at day 18 (**Fig. 4C&D**).

DV patterning of neuroepithelial cysts by RA

We next examined independent roles of RA and SHH in DV patterning of NE cysts. When only 1 μM RA was supplemented in neural induction medium from day 4 to day 9, 28.19% ± 2.31% of NE cysts achieved proper ventral patterning at day 18, with two NKX2.2+ p3 domains positioned dorsal to a single FOXA2+ FP domain (**Fig. 5A&B**). However, only 1.95% ± 0.05% of NE cysts showed PAX3-OLIG2 DV polarity, with PAX3+ dorsal cells located at the opposite pole of the OLIG2+ pMN domain (**Fig. 5A&B**). When RA concentration was reduced to 0.1 μM, no patterned NE cyst was detectable (**Fig. 5A&B**). When stimulation with 1 μM RA was prolonged from day 4

to day 18, no patterned NE cyst was detectable either at day 18 (**Fig. 5C**). FOXA2+ FP progenitor cells appeared uniformly at the cyst basal surface (**Fig. 5C**). With treated with 0.1 μM RA from Day 4 to day 18, 8.86% ± 1.18% of NE cysts showed PAX3-OLIG2 DV polarity (**Fig. 5C&D**). However, ventral patterning of NE cysts was not achieved, as even though OLIG2+ pMN domains adjacent to FOXA2+ FP domain was evident in 27.08% ± 4.45% of NE cysts, the NKX2.2 p3 domain was not detectable in any cyst (**Fig. 5C&D**). These results suggest that prolonged global RA stimulation might not be optimal for DV patterning. Together, these data suggest that optimal DV patterning of NE cysts depends on both RA concentration and the timing and duration of RA stimulation.

We next examined the independent effect of SHH. When only 10 nM SHH was supplemented in neural induction medium from day 4 to day 9, there was no distinct, localized FOXA2+ FP domain evident at day 18 (**Fig. 5E**). FOXA2 expression remained dispersed in NE cysts, with only few OLIG2+ cells randomly distributed and no NKX2.2+ cells detectable (**Fig. 5E**). We should note that a majority of cysts collapsed and contained only multiple small lumens without a single central lumen by day 18 (**Fig. S7**), suggesting that RA might have an important effect on maintaining the structural integrity of lumenal NE cysts.

To further investigate RA-mediated DV patterning of NE cysts, cyclopamine (5 μM), an inhibitor of SHH signaling, was supplemented together with RA from day 4 to day 9 (**Fig. 5F**). In the presence of cyclopamine, FOXA2+, NKX2.2+ or OLIG2+ ventral cells were undetectable at day 18, with only a few PAX3+ dorsal cells evident (**Fig. 5F**). We further performed qRT-PCR to confirm the effect of cyclopamine. With cyclopamine, *PAX3* expression was significantly upregulated, whereas expression of *OLIG2*, *NKX2.2*, *FOXA2* and *SHH* was significantly downregulated (**Fig. 5G**). Together, these data support the role of SHH signaling in the ventralizing effect of RA.

Our observation of RA-mediated DV patterning of NE cysts is consistent with previous studies on mouse NE cysts (*12, 33*), suggesting a conserved general patterning mechanism by RA.

Anterior-posterior (A-P) positional identity of neuroepithelial cysts

Previous studies have shown that prolonged dual inhibition of Activin and BMP signaling specifies hESCs towards an anterior neuroectodermal identity (*34*). Thus, NE cysts developed in Gel-3D under the neural induction condition might have an anterior identity. In addition to its role in DV patterning, RA has a posteriorizing effect on the NT *in vitro* (*35*). It is well established that RA regulates progressive HOX gene activation to establish regional identities in the posterior hindbrain and cervical spinal cord (*35*). Thus, we next evaluated the positional identity of NE cysts along the A-P axis, with or without RA supplemented in neural induction medium from day 4 to day 9 (**Fig. S8A**). qRT-PCR was conducted to assess expression of region-specific markers along the A-P axis at day 18. In RA-treated NE cysts, expression of *FOXG1* (forebrain marker), *OTX2* (forebrain / midbrain marker) and *HOXA2* (expressed in the r2 of the

hindbrain) was significantly downregulated (**Fig. S8B**). Expression of *GBX2*, a midbrain / hindbrain marker (*36*), was not affected by RA treatment (**Fig. S8B**). Expression of *HOXB4*, a cervical spinal cord marker, was significantly increased in RA-treated NE cysts (**Fig. S8B**). The anterior border of HOXB4 is at the r6/r7 boundary of hindbrain (*36*). Thus, our qRT-PCR analysis suggested that RA-treated NE cysts had a positional identity of the posterior hindbrain and the cervical spinal cord.

Generation of motor neurons from neuroepithelial cysts

After DV patterning of the NT, different progenitor domains of the NT will continue to develop and specify region-specific neuronal subtypes in each domain. The OLIG2+ pMN domain will give rise to MNs. We thus sought to specify OLIG2+ pMN progenitor cells in NE cysts into MNs. Our data in **Fig. 2D** showed an effective induction of OLIG2+ pMN progenitor cells in NE cysts by supplementing RA and SAG from day 4 to day 9 (**Fig. 6A**). Indeed, at day 9, neuronal progenitor cells with characteristic neuronal morphology and expression of neuronal markers βIII-TUBULIN and MAP2 were evident in NE cysts (**Fig. 6B**). After continuous culture of NE cysts in neural induction medium for another 9 days, by day 18, numerous neurites were evident extending into the surrounding environment from the cyst basal surface as detected by immunostaining for βIII-TUBULIN and MAP2 (**Fig. 6B**). There were a few cells even migrating out of NE cysts (**Fig. 6B**). NE cysts at day 18 contained a few cells expressing ISLET1/2 (MN-associated transcription factor); however, no HB9+ cells were detectable (HB9 is a MN-specific transcription factor), suggesting incomplete MN specification.

We next added neurotrophic factors BDNF (brain-derived neurotrophic factor; 10 ng mL^{-1}), GDNF (glial-derived neurotrophic factor; 10 ng mL^{-1}), CNTF (ciliary neurotrophic factor, 10 ng mL^{-1}), IGF-1 (insulin-like growth factor-1; 10 ng mL^{-1}), cAMP (cyclic adenosine monophosphate; 1 μM) and AA (ascorbic acid; 0.2 μg mL^{-1}) into neural induction medium from day 9 onwards (**Fig. 6C**). BDNF is a member of neurotrophin family and is required for the differentiation and survival of specific neuronal subpopulations (*37*). GDNF increases proliferation of MN progenitor cells and promotes neuronal differentiation and survival (*38*). CNTF is important for the survival of MNs (*39*), whereas IGF-1 promotes differentiation and survival of MNs (*40*). When these growth factors are used together *in vitro*, they have been shown to be effective in driving hPSC-derived neural progenitor cells into MNs (*41*). At day 18, extensive MAP2+ and βIII-TUBULIN+ neurites were evident extending from the cyst basal surface, and there were ISLET1/2+ and HB9+ neuronal cells migrating out of NE cysts (**Fig. 6D**). Importantly, there were ISLET1/2+HB9+ MNs clearly evident at the cyst peripheral region (**Fig. 6D**), suggesting successful MN specification.

ISLET1/2+HB9+ MNs are derived from the pMN domain and localized at the ventral part of the NT *in vivo*. To further examine whether ISLET1/2+HB9+ MNs developed in patterned NE cysts were derived from the pMN domain, we applied RA and SHH as DV patterning signals from day 4 to day 9 before neurotrophic factors were implemented at day 12 (**Fig. 6E**). Excitingly, at day 25, about 17% of NE cysts

contained HB9+ and ISLET1/2+ MNs at the cyst basal region adjacent to the OLIG+ pMN domain (**Fig. 6F&G**), suggesting that HB9+ and ISLET1/2+ MNs were developed from the pMN domain in NE cysts.

DISCUSSION

As the embryonic precursor to the CNS, the NT generates distinct classes of neuronal progenitor cells located at defined positions within the NT through intricate patterning events. Considerable progress has been made in determining the signaling activities and genetic networks that control region-specific neuronal fate patterning in the NT (*1, 2, 24*). It is now appreciated that acquisition of a specific neuronal fate depends on the position of precursor NE cells within the NT, which defines their exposure to inductive morphogens that gradually constrain their developmental potential in each local domain. Morphogens instructing DV patterning of the NT include WNTs, BMPs and SHH, with WNT and BMP emanated from the dorsal ectoderm and roof plate favoring dorsal identities and SHH emanated from the notochord inducing ventral identity (*1, 2, 24*). In this work, we have established the neurogenic Gel-3D culture that promotes hPSCs to self-organize into spherical, lumenal NE cysts, mimicking the development of the NT tissue *in vivo*. The intrinsic lumenogenic property of hPSCs prompt the cells to undergo lumenogenesis in Gel-3D to form a central apical lumen (*21*) (**Fig. S2**). Under the neural induction environment, hPSCs in the lumenal cyst exit pluripotency and progress long the neural lineage while continuing to divide (**Fig. S2**). By day 9, NE cysts emerge in Gel-3D, featuring a single central lumen with correct apicobasal polarity, displaying interkinetic nuclear migration and pseudostratification, and expressing early neuroectodermal markers including PAX6, SOX2, SOX1, NESTIN and N-CAD (**Fig. 1**). NE cysts at day 9 appear to correspond to an early stage of the neural plate formation in the dorsal ectoderm germ layer. Our data show that both ECM dimensionality and matrix rigidity are critical extracellular microenvironmental factors for proper development of NE cysts from hESCs. In particular, a 3D culture environment is required for the development of 3D cystic NE tissues enclosing a central lumen (**Fig. 1C**). Consistent with previous studies on mouse NE tissues (*12, 13*), hESC-derived NE cysts possess a default dorsal neural identity (**Fig. 2A&B**), supporting a conserved default dorsal neural identity of the NT for vertebrates including humans.

NE cysts derived from hPSCs in Gel-3D are responsive to morphogen stimulations (**Fig. 2C**), opening the door to modulating exogenous morphogen signals for achieving region-specific neuronal fate patterning. Excitingly, under proper DV patterning conditions, NE cells within lumenal cysts differentiate into region-specific progenitors in discrete local domains and achieve cell fate patterning along the DV axis (**Fig. 3**). Importantly, progressive development of NE cysts features sequential emergence of neural progenitor domains, with the ventral FP, P3 and pMN domains emerging progressively in discrete, non-overlapping regions and the PAX3+ dorsal territory progressively restricted to the opposite, prospective dorsal pole (**Fig. 4**). The OLIG2+ pMN domain in DV patterned NE cysts can be further specified into ISLET1/2+HB9+ MNs (**Fig. 6**).

In the Gel-3D culture, DV patterning of hESC-derived NE cysts appears to initiate after removal of exogenous morphogen signals (**Fig. 4**). This observation may be related to the hysteresis property of SHH signaling, in which intracellular SHH signaling remains active after withdrawal of exogenous morphogens (*42*). Previous studies using mouse NT explants suggest that the transcriptional network for ventral patterning of the NT can produce hysteresis, providing NE cells in the NT with a memory of SHH signaling even when extracellular signaling gradients recede (*43*). Our data further suggest a role of intracellular SHH signaling in the ventralizing effect of RA (**Fig. 5**). This observation is consistent with previous studies of the effect of RA on NE tissues derived from mouse ESCs, which have shown induction of SHH by RA administration and consequently expression of ventral NT markers (*12*). *In vivo*, both the notochord and FP secrete RA (*24*), and it has been suspected that RA may act as a permissive signal for SHH-mediated ventral patterning of the NT (*12*). Thus, it is likely that supplementation of RA in our system promotes SHH signaling, which in turn induces the specification of FOXA2+ FP progenitor cells.

It remains puzzling how global applications of exogenous morphogens lead to the formation of a local FOXA2+ FP domain. Our temporal immunofluorescence data suggest that at the initial phase of DV patterning, FOXA2+ FP progenitor cells emerge in a scattered fashion at the basal surface of NE cysts. Soon thereafter, FOXA2 expression become restricted to a local, prospective FP region at the putative ventral pole of NE cysts. This observation suggests a likely involvement of a self-enhancing activator/inhibitor signaling system, leading to a single localized FP region formation. This hypothesis remains to be validated in the future.

In this work, we have successfully derived DV patterned NT-like tissues from hPSCs. Nonetheless, it remains a significant challenge (and thus a future goal) to obtain NT-like tissues containing all progenitor domains along the DV axis. *In vivo*, DV patterning of the NT involves multiple morphogen gradients emanated from neighboring signaling centers located at different anatomical regions. Our current Gel-3D system applies global administrations of exogenous morphogens. It remains a future goal to integrate neural induction of hPSCs with advanced microfluidic systems to introduce well defined, dynamic parallel and antiparallel morphogen gradients to achieve full DV patterning of NT-like tissues. Our DV patterned NT development model offers great opportunities for experimental control of key parameters and quantitative measurements, providing a significantly advantageous experimental platform for advancing our understanding of the emergent self-organizing principles and patterning mechanisms that provide robustness and reliability to NT DV patterning, a long-standing question in biology. Patterned NT-like tissues derived from hPSCs are also useful for the development of stem-cell based regenerative therapies, disease models and screening applications for diagnosis, prevention and treatment of neurological disorders resulted from impairments of the development and growth of the CNS system.

MATERIALS AND METHODS

Cell culture. hESC line H9 (WA09, WiCell; NIH registration number: 0062), H1 (WA01, WiCell; NIH registration number: 0043) and 1196a hiPSC line (from the University of Michigan Pluripotent Stem Cell Core33) were cultured under a standard feeder-free condition in mTeSR1 medium (STEMCELL Technologies) with daily medium exchange. Cells were passaged every 5 d using dispase (STEMCELL Technologies) and the STEMPRO EZPassage Disposable Stem Cell Passaging Tool (Invitrogen). Cell pellets re-suspended in mTeSR1 were transferred onto a 6-well tissue culture plate (BD Biosciences) pre-coated with 1% lactate dehydrogenase-elevating virus (LDEV)-free hESC-qualified reduced growth factor basement membrane matrix Geltrex^{TM} (Thermo Fisher Scientific). All the cell lines used in this study had a passage number < P70, and it was authenticated as karyotypically normal by Cell Line Genetics. H9 hESC line was tested negative for mycoplasma contamination (LookOut Mycoplasma PCR Detection Kit, Sigma-Aldrich).

Fabrication of gel beds. Geltrex^{TM} gel bed was generated based on a "sandwich" scheme developed recently for inducing amniogenesis from hPSCs (*5*). In brief, two 12-mm diameter round glass coverslips were treated with air plasma (Harrick Plasma) for 2 min. One of the coverslips, which was to be coated with the gel bed, was soaked in 0.1 mg mL^{-1} poly-(L-lysine) (PLL) solution (Sigma-Aldrich) for 30 min and then in 1% glutaraldehyde solution (Electron Microscopy Sciences) for another 30 min. The other coverslip was coated with 0.1 mg mL^{-1} poly-(L-lysine)-graft-poly-(ethylene glycol) (PLL-g-PEG; SuSoS) solution for 1 h. To obtain gel beds with nominal thickness of 20, 60, and 100 μm, undiluted Geltrex (10, 30 and 50 μL, respectively) was then sandwiched between the two coverslips on ice before being incubated at 37 °C for 30 min. The glass coverslip coated with the Geltrex gel bed was then gently separated from the PLL-g-PEG coated coverslip, before being submerged in DMEM/F12 medium (Thermo Fisher Scientific) and incubated at 37 °C overnight before plating cells at the following day.

Neural induction. hESC colonies were first treated with Accutase (Sigma-Aldrich) for 10 min at 37 °C. Cells were rinsed briefly with PBS before being collected, centrifuged and re-suspended in mTeSR1 containing the ROCK inhibitor Y27632 (10 μM, Tocris). Singly dissociated hESCs were plated onto coverslips at an initial cell seeding density of 50 × 10^3 cells cm^{-2} and cultured overnight. For Gel-2D and Gel-3D cultures, the coverslip was pre-coated with the Geltrex^{TM} gel bed, whereas for Glass-2D and Glass-3D conditions, glass coverslips were pre-coated with 1% Geltrex solution for 1 h at room temperature. On the following day (day 1), culture medium was switched to fresh N2B27-based neural induction medium (see below). For Gel-3D and Glass-3D conditions, this neural induction medium contained 2% (*v* / *v*) Geltrex. Thereafter, fresh neural induction medium with or without 2% (*v* / *v*) Geltrex supplement was exchanged daily.

N2B27-based neural induction medium comprised Advance DMEM/F12 (Gibco) : Neurobasal medium (1 : 1; Gibco), 0.5× N2 (GIBCO), 0.5× B27 (GIBCO),

1× nonessential amino acids (GIBCO), 2 mM L-glutamine (GIBCO) and 0.1 mM b-mercaptoethanol (Sigma). N2B27-based neural induction medium further contained TGF-β pathway inhibitor SB431542 (SB, 10 μM; STEMCELL Technologies) and BMP inhibitor LDN193189 (LDN, 0.1 μM; STEMCELL Technologies).

For dorsalization of neuroepithelial cysts, 3 μM CHIR99021 (CHIR; STEMCELL Technologies) was supplemented into neural induction medium from day 4 to day 9. For ventralization of neuroepithelial cysts, all-trans retinoic acid (RA, 1 μM; TEMCELL Technologies), recombinant human Sonic Hedgehog (SHH, 10 nM or 100 nM; PeproTech), and / or smoothened agonist (SAG, 1 μM; STEMCELL Technologies) were supplemented into neural induction medium from day 4. For motor neuron induction, the following chemicals were added to neural induction medium from day 9 or day 12: 10 ng mL^{-1} brain-derived neurotrophic factor (BDNF; R&D systems), 10 ng mL^{-1} glial-derived neurotrophic factor (GDNF; PeproTech), 10 ng mL^{-1} ciliary neurotrophic factor (CNTF; PeproTech) 10 ng mL^{-1} insulin-like growth factor-1 (IGF-1; PeproTech), 1 μM cyclic adenosine monophosphate (cAMP; Sigma), and 0.2 μg mL^{-1} ascorbic acid (Sigma).

Immunocytochemistry. Cystic tissues were fixed in 4% paraformaldehyde (PFA, Electron Microscopy Sciences) at room temperature for 1 h before being permeabilized with 0.1% sodium dodecyl sulfate (SDS, dissolved in PBS) solution at room temperature for 3 h. Cysts were then blocked in 10% goat serum solution (Thermo Fisher Scientific) or 4% donkey serum solution (Sigma) at 4 °C overnight. Immunostaining was performed in primary antibody solutions prepared in blocking buffer for 24 h at 4 °C. Cysts were then washed with PBS and incubated with goat- or donkey-raised secondary antibodies at 4 °C for another 24 h. DAPI (Invitrogen) was used for counterstaining cell nuclei. All primary antibodies, their sources and dilutions are listed in **Supplementary Table 1**. For 5-ethynyl-20-deoxyuridine (EdU) incorporation, neuroepithelial cysts at day 8 were incubated with EdU for 1 h and fixed thereafter. EdU was detected using the Click-iT EdU Alexa Fluor 488 Imaging Kit (Thermo Fisher Scientific).

Quantitative real-time PCR (qRT-PCR) analysis. Total RNA was isolated from untreated hESCs or neuroepithelial cysts using the RNeasy Micro Kit (QIAGEN). RNA quality and concentration were detected using the NanoDrop 1000 spectrophotometer (Thermo Scientific). RNA was reverse transcribed with the iScript cDNA synthesis Kit (Bio-Rad). qRT-PCR was performed with Quantitect Sybr Green MasterMix (QIAGEN) and gene specific primers on the CFX Connect Real-Time System (Bio-Rad). Human GAPDH was used as an endogenous control for quantifying relative gene expression by calculating $2^{-\Delta\Delta Ct}$ with the corresponding s.e.m. All analyses were performed with at least three biological replicates. Primers used in this work are listed in **Supplementary Table 2**.

Confocal microscopy and image analysis. Images were recorded using an Olympus 1×81 fluorescence microscope with a CSU-X1 spinning-disc unit (YOKOGAWA). 3D reconstructed cyst images were obtained using ImageJ (NIH).

Western blotting. Whole-cell lysates were extracted from cells before being homogenized by sonication. SDS-polyacrylamide gel electrophoresis (SDS-PAGE) was employed for separation of proteins, which were then transferred onto PVDF membranes. PVDF membranes were incubated with blocking buffer (Li-Cor) for 3 h and then with primary antibodies (**Supplementary Table 1**) overnight at 4 °C. Blots were incubated with IRDye secondary antibodies (Li-Cor) for 3 h at room temperature. Protein expression was detected by the Li-Cor Odyssey Sa Infrared Imaging System (Li-Cor).

Statistical analysis. All data are shown as the mean ± s.e.m. Statistical analysis on the qRT-PCR data was performed using two-side unpaired student *t*-tests in Excel (Microsoft). $P < 0.05$ was considered statistically significant

ACKNOWLEDGEMENT

This work was supported by the University of Michigan Mechanical Engineering Faculty Support Fund (J.F.), the Michigan-Cambridge Research Initiative (J.F.), and the University of Michigan Mcubed Fund (J.F.). A. M. Resto Irizarry is partially supported by the National Science Foundation Graduate Research Fellowship under Grant No. DGE 1256260.

COMPETING INTERESTS

The authors declare that they have no competing interests.

AUTHOR CONTRIBUTIONS

Y.Z. (Yuanyuan Zheng), G.Z. and J.F. conceived and initiated the project; Y.Z. (Yuanyuan Zheng) and X.X. designed, performed and analyzed most of experiments; A.M.R.I., Z.L., Y.S. and Y.Z. (Yi Zheng) helped design and perform experiments and image and data analyses; Y.Z. (Yuanyuan Zheng), X.X., G.Z. and J.F. wrote the manuscript; G.Z. and J.F. supervised the study. All authors edited and approved the manuscript.

DATA AND MATERIALS AVAILABILITY

All data needed to evaluate the conclusions in the paper are present in the paper and/or the Supplementary Materials. Additional data related to this paper may be requested

from the authors.

SUPPLEMENTARY MATERIALS

Figures: S1-S8

Tables: Table 1 and Table 2

REFERENCES

1. T. M. Jessell, Neuronal specification in the spinal cord: Inductive signals and transcriptional codes. *Nature Reviews Genetics* **1**, 20-29 (2000).
2. J. Briscoe, S. Small, Morphogen rules: Design principles of gradient-mediated embryo patterning. *Development* **142**, 3996-4009 (2015).
3. D. M. Juriloff, M. J. Harris, Mouse models for neural tube closure defects. *Hum Mol Genet* **9**, 993-1000 (2000).
4. A. Warmflash, B. Sorre, F. Etoc, E. D. Siggia, A. H. Brivanlou, A method to recapitulate early embryonic spatial patterning in human embryonic stem cells. *Nature Methods* **11**, 847-854 (2014).
5. Y. Shao *et al.*, A pluripotent stem cell-based model for post-implantation human amniotic sac development. *Nature Communications* **8**, 208 (2017).
6. X. Xue *et al.*, Mechanics-guided embryonic patterning of neuroectoderm tissue from human pluripotent stem cells. *Nature Materials* **17**, 633-641 (2018).
7. T. Haremaki *et al.*, Self-organizing neuruloids model developmental aspects of Huntington's disease in the ectodermal compartment. *Nature Biotechnology* **37**, 1198-1208 (2019).
8. M. Simunovic *et al.*, A 3D model of a human epiblast reveals BMP4-driven symmetry breaking. *Nature Cell Biology* **21**, 900-910 (2019).
9. Y. Zheng *et al.*, Controlled modelling of human epiblast and amnion development using stem cells. *Nature* **573**, 421-425 (2019).
10. P. Itsykson *et al.*, Derivation of neural precursors from human embryonic stem cells in the presence of noggin. *Mol Cell Neurosci* **30**, 24-36 (2005).
11. M. A. Lancaster *et al.*, Cerebral organoids model human brain development and microcephaly. *Nature* **501**, 373-379 (2013).
12. A. Meinhardt *et al.*, 3D reconstitution of the patterned neural tube from embryonic stem cells. *Stem Cell Rep* **3**, 987-999 (2014).
13. A. Ranga *et al.*, Neural tube morphogenesis in synthetic 3D microenvironments. *Proc Natl Acad Sci U S A* **113**, E6831-E6839 (2016).
14. T. Ogura, H. Sakaguchi, S. Miyamoto, J. Takahashi, Three-dimensional induction of dorsal, intermediate and ventral spinal cord tissues from human pluripotent stem cells. *Development* **145**, dev162214 (2018).
15. J. T. Paridaen, W. B. Huttner, Neurogenesis during development of the vertebrate central nervous system. *EMBO Rep* **15**, 351-364 (2014).
16. Y. Sun *et al.*, Hippo/YAP-mediated rigidity-dependent motor neuron differentiation of human pluripotent stem cells. *Nat Mater* **13**, 599-604 (2014).
17. S. M. Chambers *et al.*, Highly efficient neural conversion of human ES and iPS cells by dual inhibition of SMAD signaling. *Nature Biotechnology* **27**, 275-280 (2009).
18. Y. Shao *et al.*, Self-organized amniogenesis by human pluripotent stem cells in a biomimetic implantation-like niche. *Nature Materials* **16**, 419-425 (2017).
19. M. T. Pankratz *et al.*, Directed neural differentiation of human embryonic stem cells via an obligated primitive anterior stage. *Stem Cells* **25**, 1511-1520 (2007).
20. X. Q. Zhang *et al.*, Pax6 is a human neuroectoderm cell fate determinant. *Cell*

682 *Stem Cell* **7**, 90-100 (2010).
683 21. K. Taniguchi *et al.*, Lumen formation is an intrinsic property of isolated human
684 pluripotent stem cells. *Stem Cell Rep* **5**, 954-962 (2015).
685 22. K. F. Liem, G. Tremml, H. Roelink, T. M. Jessell, Dorsal differentiation of
686 neural plate cells induced by BMP-mediated signals from epidermal ectoderm.
687 *Cell* **82**, 969-979 (1995).
688 23. J. Tailor *et al.*, Stem cells expanded from the human embryonic hindbrain stably
689 retain regional specification and high neurogenic potency. *J Neurosci* **33**,
690 12407-12422 (2013).
691 24. C. Kiecker, A. Lumsden, The role of organizers in patterning the nervous system.
692 *Annu Rev Neurosci* **35**, 347-367 (2012).
693 25. R. Alvarez-Medina, J. Cayuso, T. Okubo, S. Takada, E. Marti, Wnt canonical
694 pathway restricts graded Shh/Gli patterning activity through the regulation of
695 Gli3 expression. *Development* **135**, 237-247 (2008).
696 26. K. Yu, S. McGlynn, M. P. Matise, Floor plate-derived sonic hedgehog regulates
697 glial and ependymal cell fates in the developing spinal cord. *Development* **140**,
698 1594-1604 (2013).
699 27. X. J. Li *et al.*, Directed differentiation of ventral spinal progenitors and motor
700 neurons from human embryonic stem cells by small molecules. *Stem Cells* **26**,
701 886-893 (2008).
702 28. M. E. Hester *et al.*, Rapid and efficient generation of functional motor neurons
703 from human pluripotent stem cells using gene delivered transcription factor
704 codes. *Mol Ther* **19**, 1905-1912 (2011).
705 29. H. W. M. Vanstraaten, J. W. M. Hekking, E. J. L. M. Wiertzhoessels, F. Thors,
706 J. Drukker, Effect of the notochord on the differentiation of a floor plate area in
707 the neural-tube of the chick-embryo. *Anat Embryol* **177**, 317-324 (1988).
708 30. E. Dessaud, A. P. McMahon, J. Briscoe, Pattern formation in the vertebrate
709 neural tube: a sonic hedgehog morphogen-regulated transcriptional network.
710 *Development* **135**, 2489-2503 (2008).
711 31. J. Briscoe, A. Pierani, T. M. Jessell, J. Ericson, A homeodomain protein code
712 specifies progenitor cell identity and neuronal fate in the ventral neural tube.
713 *Cell* **101**, 435-445 (2000).
714 32. G. Le Dreau, E. Marti, Dorsal-ventral patterning of the neural tube: a tale of
715 three signals. *Dev Neurobiol* **72**, 1471-1481 (2012).
716 33. Y. Okada, T. Shimazaki, G. Sobue, H. Okano, Retinoic-acid-concentration-
717 dependent acquisition of neural cell identity during in vitro differentiation of
718 mouse embryonic stem cells. *Dev Biol* **275**, 124-142 (2004).
719 34. B. Surmacz *et al.*, Directing differentiation of human embryonic stem cells
720 toward anterior neural ectoderm using small molecules. *Stem Cells* **30**, 1875-
721 1884 (2012).
722 35. M. Maden, Retinoids and spinal cord development. *J Neurobiol* **66**, 726-738
723 (2006).
724 36. C. Nolte, R. Krumlauf, in *HOX gene expression*. (Springer, 2007), pp. 14-41.
725 37. I. Faravelli *et al.*, Motor neuron derivation from human embryonic and induced

pluripotent stem cells: experimental approaches and clinical perspectives. *Stem Cell Res Ther* **5**, 87 (2014).
38. L. Minichiello, R. Klein, TrkB and TrkC neurotrophin receptors cooperate in promoting survival of hippocampal and cerebellar granule neurons. *Gene Dev* **10**, 2849-2858 (1996).
39. S. Schaller *et al.*, Novel combinatorial screening identifies neurotrophic factors for selective classes of motor neurons. *Proceedings of the National Academy of Sciences* **114**, E2486-E2493 (2017).
40. C. Bardy *et al.*, Neuronal medium that supports basic synaptic functions and activity of human neurons in vitro. *P Natl Acad Sci USA* **112**, E3312-E3312 (2015).
41. D. Cortes *et al.*, Transgenic GDNF positively influences proliferation, differentiation, maturation and survival of motor neurons produced from mouse embryonic stem cells. *Front Cell Neurosci* **10**, 217 (2016).
42. B. D. Harfe *et al.*, Evidence for an expansion-based temporal Shh gradient in specifying vertebrate digit identities. *Cell* **118**, 517-528 (2004).
43. N. Balaskas *et al.*, Gene regulatory logic for reading the Sonic Hedgehog signaling gradient in the vertebrate neural tube. *Cell* **148**, 273-284 (2012).

FIGURE LEGENDS

Figure 1. hESCs form neuroepithelial (NE) cysts in an engineered 3D neurogenic niche. (**A&B**) Schematic of neural induction in a 3D *in vitro* culture system comprising a gel bed and an ECM overlay (Gel-3D). For comparison, culture systems were generated without gel bed but with ECM overlay (Glass-3D), or with gel bed but without ECM overlay (Gel-2D), or without either gel bed or ECM overlay (Glass-2D). (**C**) Representative confocal micrographs showing multicellular structures at day 8 under different culture conditions as indicated stained for PAX6 and N-CAD. DAPI counterstained nuclei. (**D**) Representative cystic tissues in Gel-3D at day 8 stained for PAX6, NESTIN, SOX2, N-CAD, SOX17, BRACHYURY, CDX2 and EOMES as indicated. DAPI counterstained nuclei. (**E**) Representative cystic tissues in Gel-3D at day 13 stained for ZO-1 and SOX1 as indicated. DAPI counterstained nuclei. (**F**) Representative cystic tissues in Gel-3D at day 8 stained for EdU and phospho-histone H3 (pH3) as indicated. DAPI counterstained nuclei. $n = 3$ independent experiments. Scale bars in C-F, 50 μm.

Figure 2. Dorsalization and ventralization of neuroepithelial (NE) cysts in Gel-3D. (A) NE cysts obtained at day 9 and day 18 under neural induction condition as indicated. Bright field images show representative cyst morphologies. (**B**) Representative confocal micrographs show NE cysts obtained at day 9 and day 18 stained for PAX3, PAX6, MSX1, FOXA2, OLIG2 and NKX2.2 as indicated. DAPI counterstained nuclei. (**C**) Dorsalization with CHIR99021 (CHIR) and ventralization with smoothened agonist (SAG), or retinoic acid (RA) and SAG, or RA, SAG and sonic hedgehog (SHH), from day 4 to day 9. Bright field images show representative NE cyst morphologies at day 9. (**D**) Representative confocal micrographs showing cysts at day 9 stained for PAX3, PAX6, MSX1, FOXA2, OLIG2 and NKX2.2 as indicated. DAPI counterstained nuclei. $n = 3$ independent experiments. Scale bars in A & C, 200 μm. Scale bars in B & D, 50 μm.

Figure 3. Self-organized, emergent dorsal-ventral (DV) patterning of neuroepithelial (NE) cysts in Gel-3D. (**A**) Schematic of patterning of NE cysts with RA and SAG or RA and SHH from day 4 to day 9. (**B&C**) Representative confocal micrographs showing RA/SAG-treated NE cysts at day 18 stained for dorsal and ventral markers as indicated (B). C plots percentages of different patterned cysts. (**D-F**) Representative confocal micrographs showing RA/SHH-treated NE cysts at day 18 stained for dorsal and ventral markers as indicated (D: SHH, 10 nM; E: SHH, 100 nM). F plots percentages of different patterned cysts under indicated conditions. Data in C&F represent the mean ± s.e.m. A total of 150 cysts was pooled from $n = 3$ independent experiments under both RA/SAG and RA/SHH conditions. Scale bars in B, D & E, 50 μm.

Figure 4. Dynamics of dorsal-ventral patterning of neuroepithelial cysts in Gel-3D.

(**A**) Representative confocal micrographs showing cysts stained for PAX3 and OLIG2 at different days as indicated. (**B**) Pie charts showing percentages of different types of cysts at different days as indicated. Cysts were grouped into 5 categories as indicated (PAX3+OLIG2-, PAX3-OLIG2-, PAX3+OLIG2+ patterned, PAX3+OLIG2+ unpatterned, PAX3-OLIG2+). (**C**) Representative confocal micrographs showing cysts stained for NKX2.2 and FOXA2 at different days as indicated. (**D**) Pie charts showing percentages of different types of cysts at different days as indicated. Cysts were grouped into 5 categories as indicated (NKX2.2-FOXA2+, NKX2.2-FOXA2-, NKX2.2+FOXA2+ patterned, NKX2.2+FOXA2+ unpatterned, NKX2.2+FOXA2-). Data in B & D represent the mean. A total of 150 cysts was counted from $n = 3$ independent experiments at each time point. Scale bars in A & C, 50 μm.

Figure 5. Independent effects of RA and SHH on patterning of neuroepithelial (NE) cysts in Gel-3D. (**A**) Effect of RA stimulation (1 μM or 0.1 μM) alone from day 4 to day 9. Representative confocal micrographs show cysts at day 18 stained for dorsal and ventral markers as indicated. (**B**) Percentages of different patterned cysts as a function of RA dose. Data represent the mean ± s.e.m. A total of 150 cysts was counted from $n = 3$ independent experiments at each RA dose. (**C**) Effect of RA stimulation (1 μM or 0.1 μM) alone from day 4 to day 18. Representative confocal micrographs show cysts at day 18 stained for dorsal and ventral markers as indicated. (**D**) Percentages of different patterned cysts as a function of RA dose. Data represent the mean ± s.e.m. 50 cysts were counted from each independent experiment. $n = 3$ independent experiments at each RA dose. (**E**) Effect of SHH stimulation alone from day 4 to day 9. Representative confocal micrographs show cysts at day 18 stained for dorsal and ventral markers as indicated. (**F**) Effect of inhibition of SHH signaling with cyclopamine from day 4 to day 9. Representative confocal micrographs show cysts at day 18 stained for dorsal and ventral markers as indicated. (**G**) qRT-PCR analysis of *PAX3*, *OLIG2*, *NKX2.2*, *FOXA2* and *SHH* expression for cysts at day 18 with or without cyclopamine treatment. Data are normalized against GAPDH and represent the mean ± s.e.m. $n = 3$ independent experiments. *P*-values were calculated using unpaired, two-tailed student's *t*-test. *, $P < 0.05$; **: $P < 0.01$; ***, $P < 0.001$. Scale bars in A, C, D & E, 50 μm.

Figure 6. Induction of spinal motor neurons (MNs) from neuroepithelial (NE) cysts in Gel-3D. (**A&B**) Induction of spinal MNs with RA and SAG supplemented from day 4 to day 9. Representative confocal micrographs in B show cysts at day 9 and day 18 stained for βIII-TUBULIN, MAP2, ISLET1/2 and HB9 as indicated. DAPI counterstained nuclei. (**C&D**) Induction of spinal MNs with RA and SAG supplemented from day 4 to day 9 and neurotrophic factors brain-derived neurotrophic factor (BDNF), glial-derived neurotrophic factor (GDNF), ciliary neurotrophic factor (CNTF), insulin-like growth factor-1 (IGF-1), cyclic adenosine monophosphate (cAMP) and ascorbic acid (AA) supplemented from day 9 to day 18. Representative confocal micrographs in D show cysts at day 18 stained for ISLET1/2, MAP2, HB9 and βIII-TUBULIN as indicated. DAPI counterstained nuclei. The zoomed-in image shows a

magnified view of the area highlighted by the white square. (**E&F**) Induction of spinal MNs with RA and SHH supplemented from day 4 to day 9 and neurotrophic factors from day 12 to day 25. Representative confocal micrographs in F show cysts at day 25 stained for FOXA2, OLIG2, HB8 and ISLET1/2. (**G**) Percentage of different patterned cysts. Data represent the mean ± s.e.m. n_{cyst} = 126 and 134 for HB9 staining and ISLET1/2 staining, respectively. n = 3 independent experiments. Scale bars in B, D & F, 50 μm.

FIGURES AND LEGENDS

Figure 1

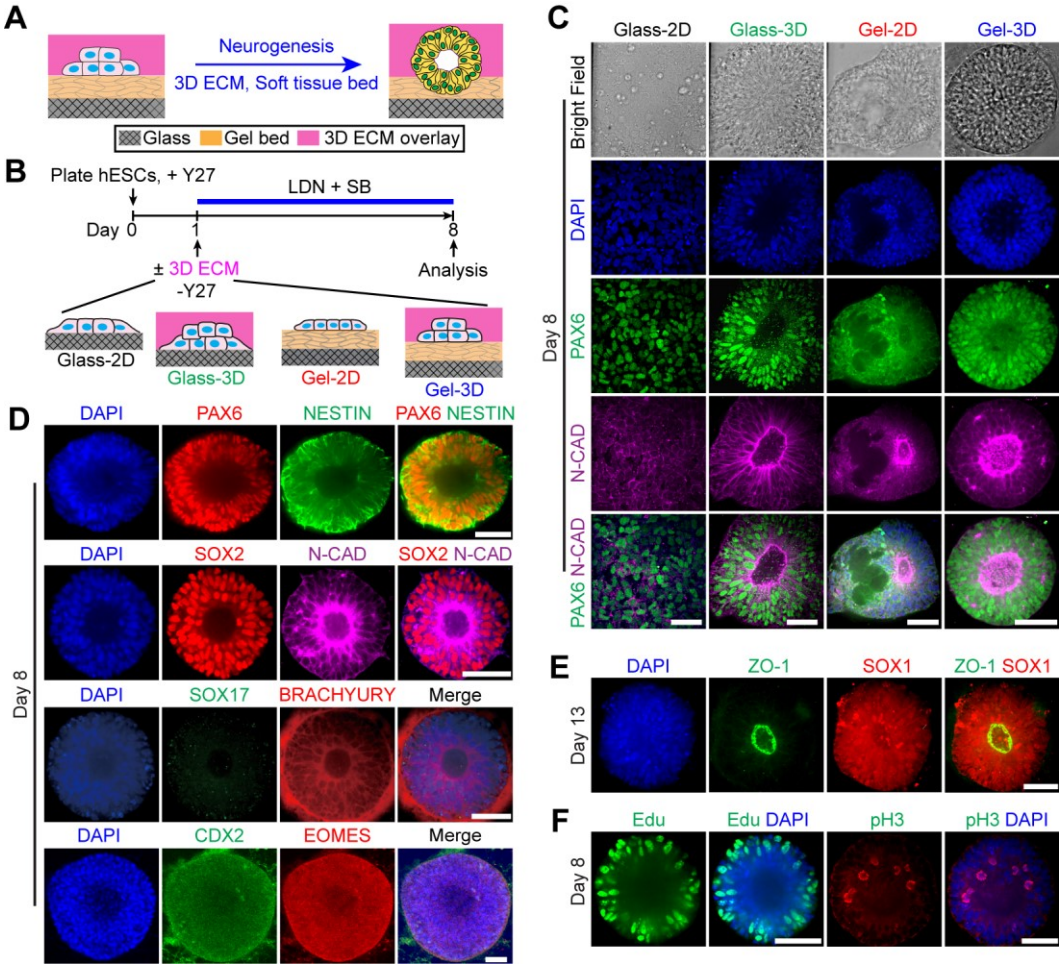

846 **Figure 2**

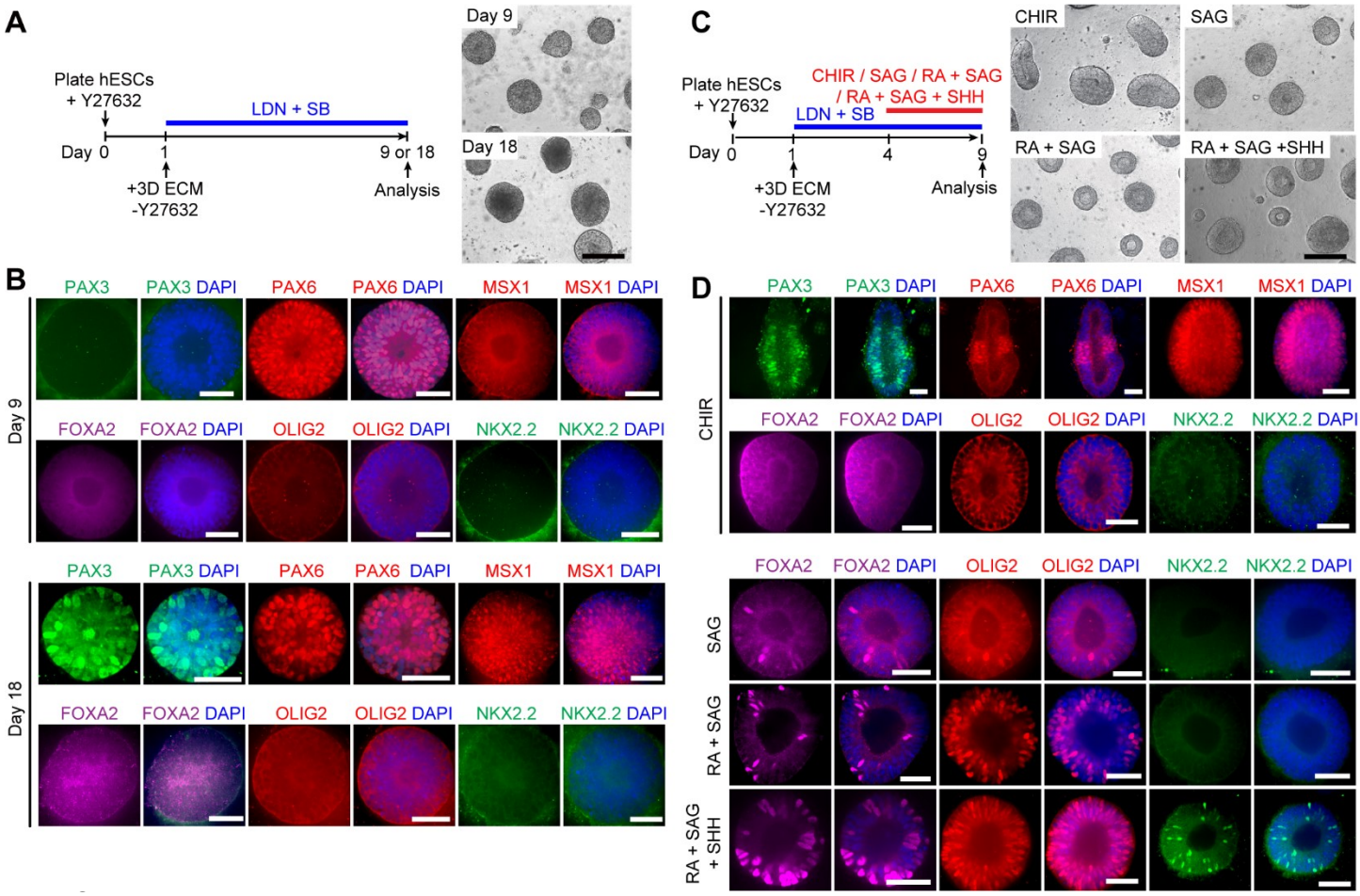

848

Figure 3

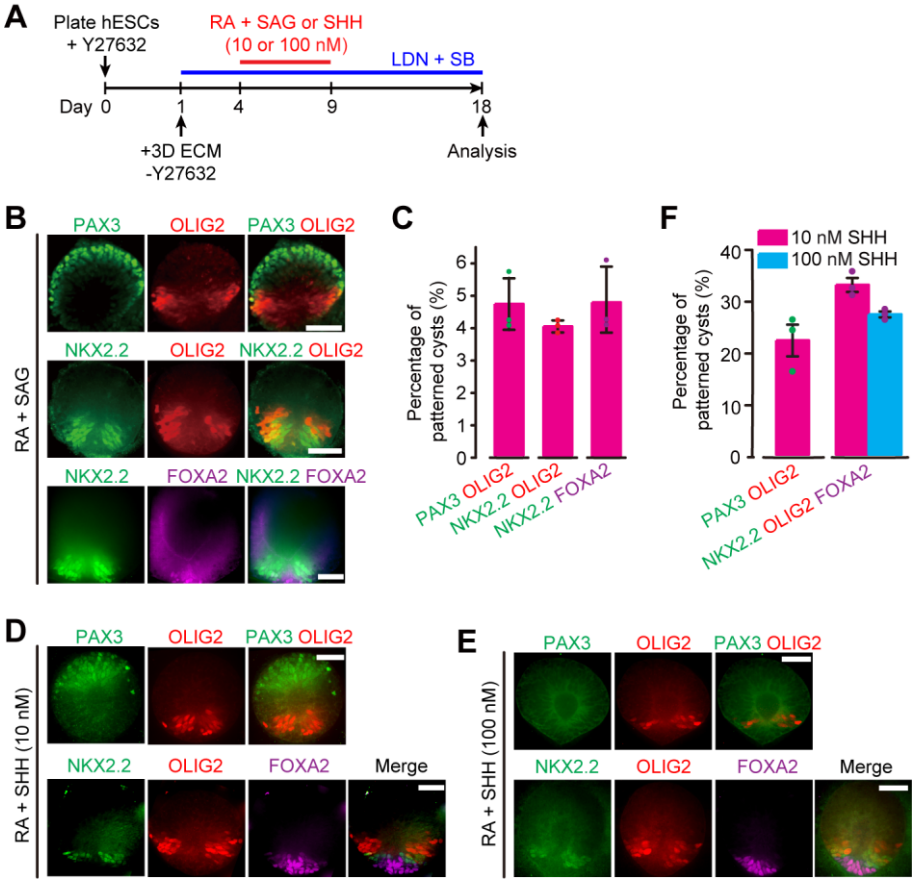
A
Plate hESCs
+ Y27632
RA + SAG or SHH
(10 or 100 nM)
LDN + SB
Day 0
1
4
9
18
+3D ECM
-Y27632
Analysis
B
PAX3
OLIG2
PAX3 OLIG2
NKX2.2
OLIG2
NKX2.2 OLIG2
NKX2.2
FOXA2
NKX2.2 FOXA2
RA + SAG
C
Percentage of patterned cysts (%)
PAX3 OLIG2
NKX2.2 OLIG2
NKX2.2 FOXA2
F
10 nM SHH
100 nM SHH
Percentage of patterned cysts (%)
PAX3 OLIG2
NKX2.2 OLIG2 FOXA2
D
PAX3
OLIG2
PAX3 OLIG2
NKX2.2
OLIG2
FOXA2
Merge
RA + SHH (10 nM)
E
PAX3
OLIG2
PAX3 OLIG2
NKX2.2
OLIG2
FOXA2
Merge
RA + SHH (100 nM)

853 **Figure 4**

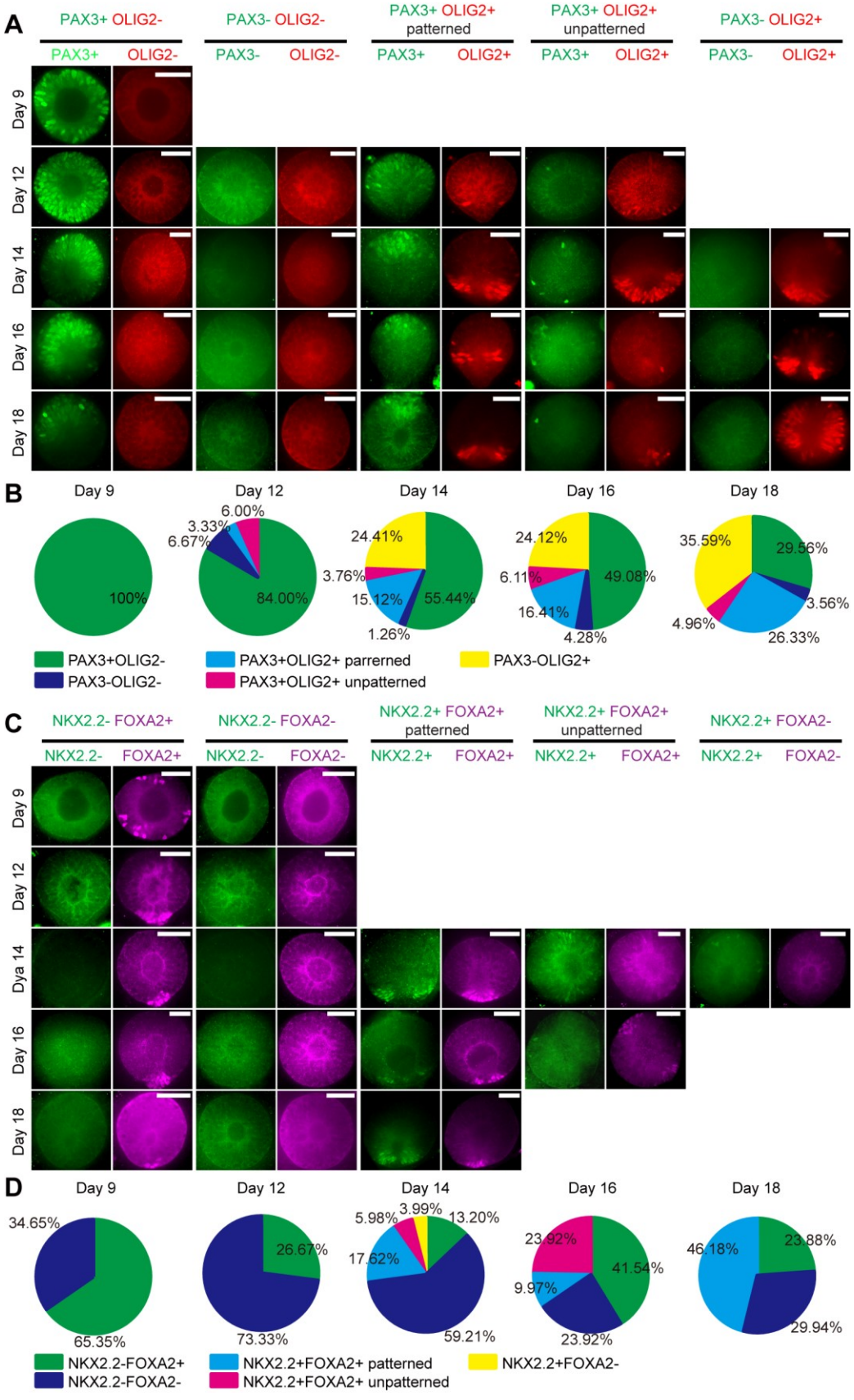

854

855 .

856

857 **Figure 5**

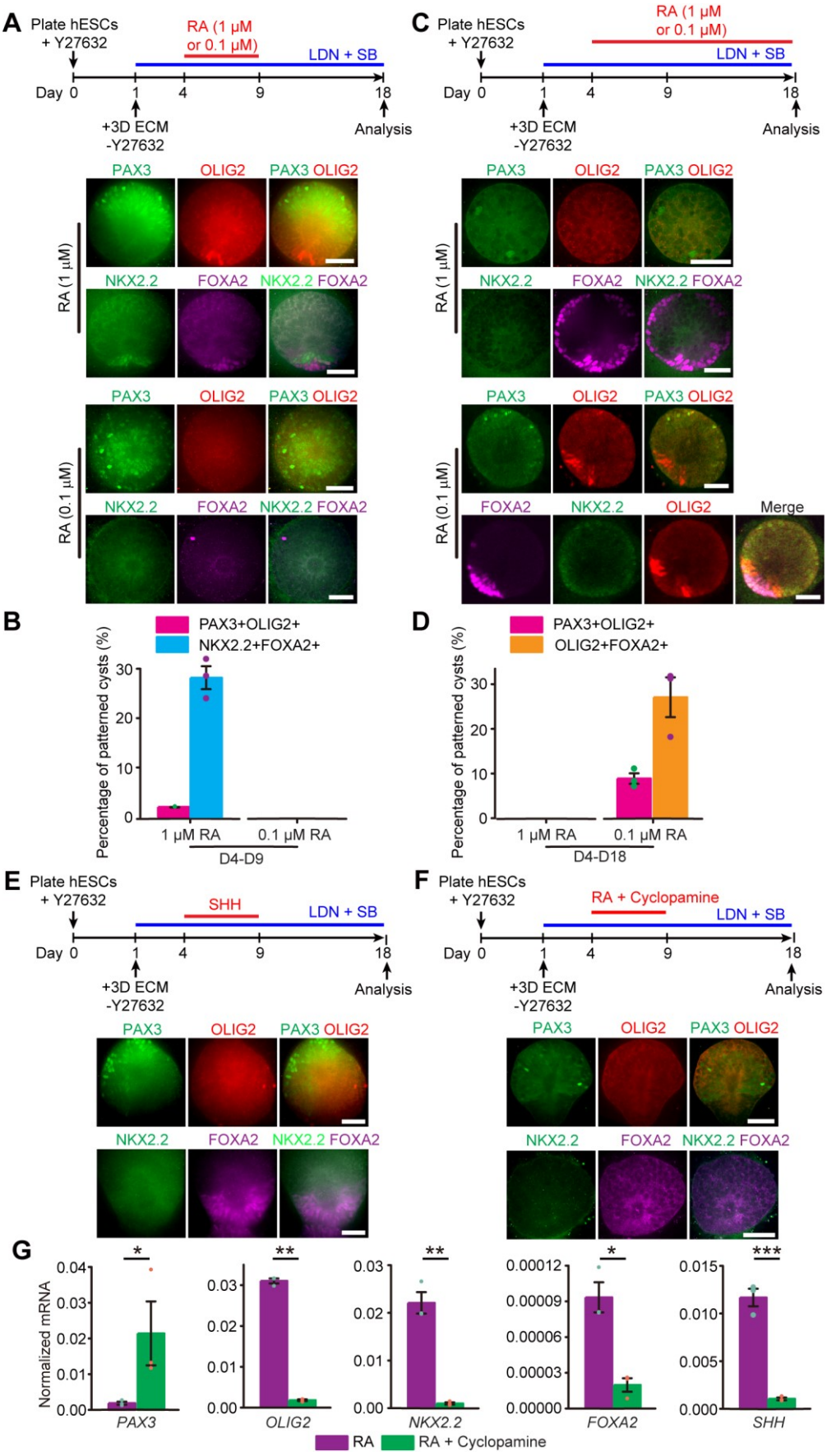

858

859

Figure 6

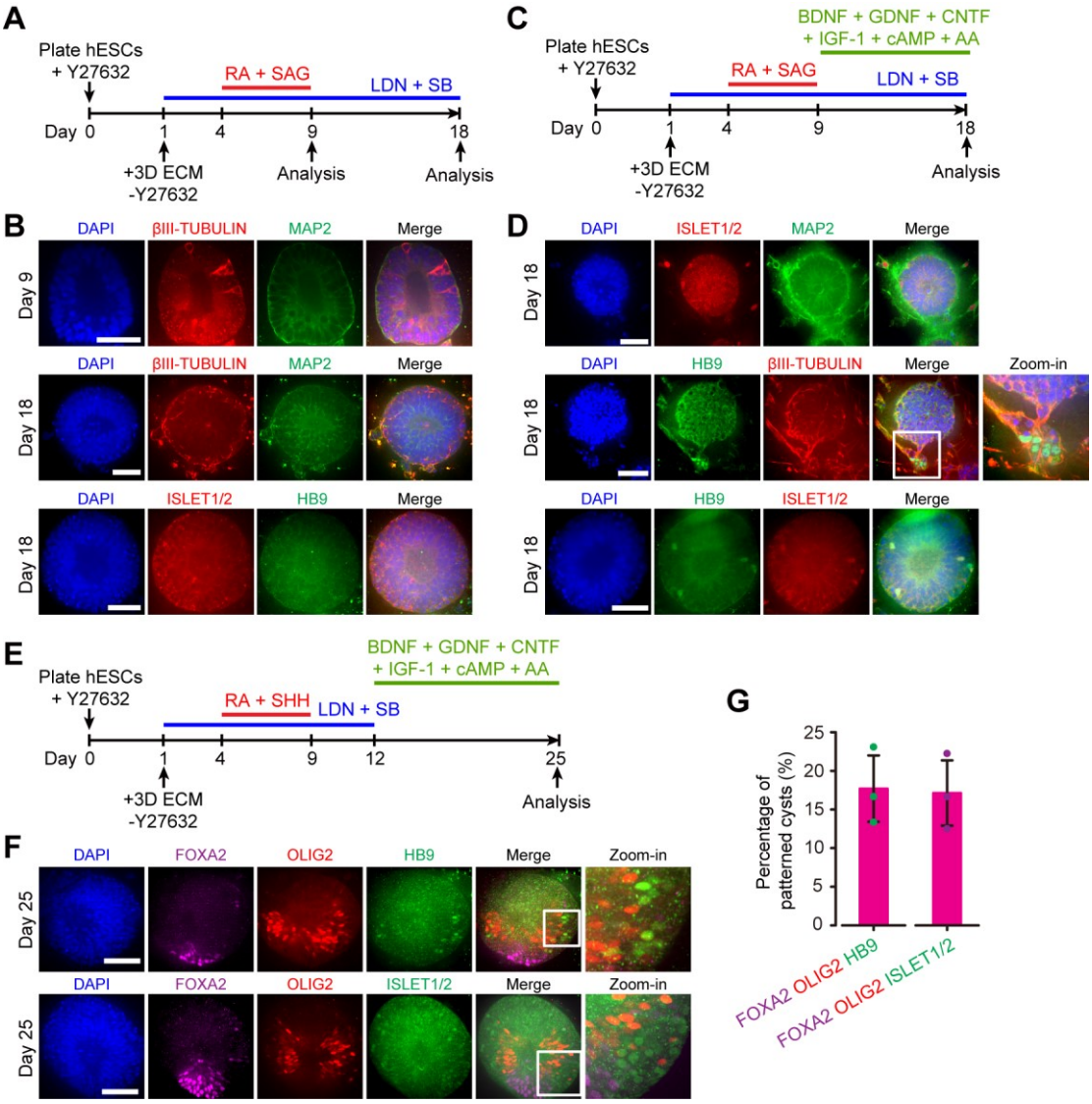
A
Plate hESCs
+ Y27632
RA + SAG
LDN + SB
Day 0
1
4
9
18
+3D ECM
-Y27632
Analysis
Analysis
C
BDNF + GDNF + CNTF
+ IGF-1 + cAMP + AA
Plate hESCs
+ Y27632
RA + SAG
LDN + SB
Day 0
1
4
9
18
+3D ECM
-Y27632
Analysis
B
DAPI
βIII-TUBULIN
MAP2
Merge
Day 9
Day 18
Day 18
Day 18
D
DAPI
ISLET1/2
MAP2
Merge
Day 18
DAPI
HB9
βIII-TUBULIN
Merge
Zoom-in
Day 18
DAPI
HB9
ISLET1/2
Merge
Day 18
E
BDNF + GDNF + CNTF
+ IGF-1 + cAMP + AA
Plate hESCs
+ Y27632
RA + SHH
LDN + SB
Day 0
1
4
9
12
25
+3D ECM
-Y27632
Analysis
F
DAPI
FOXA2
OLIG2
HB9
Merge
Zoom-in
Day 25
DAPI
FOXA2
OLIG2
ISLET1/2
Merge
Zoom-in
Day 25
G
Percentage of patterned cysts (%)
25
20
15
10
5
0
FOXA2 OLIG2 HB9
FOXA2 OLIG2 ISLET1/2